Chapter 5

General analysis tools

Along the 12 years of the ALEPH data taking, many analysis tools have been developed and improved, to serve general purposes, such as lepton identification and vertex finding. In this Chapter, those analysis tools used in the work presented in this thesis are described. In the first Section, the criteria to select events with a Z-boson decaying into a $q\overline{q}$ pair are explained. The three jet clustering algorithms used in this thesis are introduced in Section 5.2. In Section 5.3, the electron and muon identification procedures are described. The primary vertex finding method is explained in Section 5.4, and the procedure to estimate the track impact parameter is discussed in Section 5.5. Although the final secondary vertex algorithm used in the inclusive semileptonic analysis in Chapter 6 is an original work of mine (described later in Section 6.3), it uses, as a first step, the result of a standard inclusive secondary vertex finder. Two such vertex finders are available in ALEPH, both of them are described in Section 5.6. The last Section of this Chapter is dedicated to the general tools for the selection of events which contain b-hadron decays. The method used in the thesis for b-tagging was especially developed for it, however, the three b-tagging tools described in Section 5.7 are used, together with other information, as explained later in Section 6.4.

5.1 Hadronic selection

Hadronic events, *i.e.*, originating from $Z \to q\overline{q}$ decays, are selected using charged particle information alone. At least five charged particle tracks must be reconstructed by the TPC for an event to be selected. These tracks need to satisfy the following requirements to be called "good tracks". *i*) Four or more TPC three-dimensional points must be used for the track helix fit; *ii*) the track must originate from a cylinder centred in the beam position, with radius 2 cm and length 10 cm; and *iii*) the track polar angle with the beam axis must satisfy $|\cos\theta| < 0.95$, to ensure that six or more pad rows in the TPC are hit.

A cut on the total measured charged energy is applied in order to remove events for which the hadronic final state is less likely to come from a Z-boson decay than from the interaction of two photons radiated from the incident e^+e^-. The sum of the momenta of all good tracks is required to exceed 10% of the centre-of-mass energy. This cut also removes efficiently events produced by beam-gas interactions. The total efficiency of this selection is 97.48% [69], the

losses originating mainly from events at low polar angle. This selection is especially interesting because its systematic uncertainties are well under control and only account for 0.087%; the dominant background for this selection (which is anyway negligible once combined with other selection criteria like it is done in Chapter 6) comes from $e^+e^- \to \tau^+\tau^-$ and two photon interactions with a hadronic final state. Another good feature of the selection is that it is independent of the quark flavour to better than 0.1%.

The *thrust* axis of an event is defined as a vector $\vec{n}$ such that the quantity T defined as,

$$T \equiv \frac{\sum_{i=1}^{N} |\vec{p_i} \cdot \vec{n}|}{\sum_{i=1}^{N} |\vec{p_i}|} , \tag{5.1}$$

is maximal, where, $\vec{p_i}$ is the momentum of the i-th particle and N is the total number of reconstructed particles (charged and neutral) in the event (see Section 4.2.3). This direction aims at the reconstruction of the direction of the quarks from the Z decay. However, in the case of a hard gluon radiation, $Z \to q\overline{q}g$, this intuitive meaning is lost.

The thrust axis is therefore used to divide the event into two hemispheres with respect to the plane perpendicular to $\vec{n}$ and including the interaction point. With this definition, each hemisphere contains the fragmentation and hadronization products of each of the quarks from the Z decay (except in some rare cases of $Z \to q\overline{q}g$ decay) .

5.2 Jet algorithms

At high energy (approximately above 20 GeV or so), quarks and gluons are produced with a boost large enough to form "jets" of particles from their hadronization.

Three different jet clustering algorithms are used for the analyses described in this thesis. They are described in the following subsections.

5.2.1 The JADE algorithm

The JADE algorithm is described in Ref. [71]. In each event, charged and neutral particles are clustered in jets with the following prescription. Two particles are grouped together if the distance y_{ij} defined as

$$y_{ij} = \frac{2E_iE_j\,(1-\cos\theta_{ij})}{E_{\rm vis}^2} , \tag{5.2}$$

is smaller than a predefined cut value called the jet-resolution parameter, $y_{\rm cut}$. In Eq. 5.2, E_i and E_j are the energies of particles i and j, θ_{ij} is the angle between the momenta of these particles, and $E_{\rm vis}$ is an estimate of the total visible energy in the event. The numerator in Eq. 5.2 is equal to m_{ij}^2, the invariant mass of the system, if particles i and j are considered massless. The particle pair with the smallest value of y_{ij} is kept, the two original particles are replaced by a new pseudo-track, the energy and momentum of which is obtained from

the sum of energy and momenta of the two parent particles. The same procedure is repeated until no pair which fulfils $y_{ij} \leq y_{\rm cut}$ is found. The pseudo-tracks obtained at the last step are the particle jets.

5.2.2 The Nucleated jet algorithm

In the Nucleated jet algorithm [72], the jet is built around an *a priori* track seed (the choice of this charged particle depends on the data analysis to be performed). The quadri-momenta of charged and neutral particles close to the chosen seed are added until the mass of the jet reaches a cut value $m_{\rm cut}$, which has to be optimized depending on the type of jet to be reconstructed (from a b- or c-hadron, for instance). The criterion for a "close" particle is the same as in the JADE algorithm above. In the analysis described in Chapter 6, this algorithm is used to reconstruct the charmed object momentum. In order to reject tracks not originating from the b-hadron decay, particles with momentum smaller than $500\,\mathrm{MeV}/c$ are excluded from the the clustering process.

5.2.3 A cone algorithm: BTCONE

In a cone algorithm, particles are grouped together according to their angular proximity. A track is taken as a seed (the seed choice depends on the data analysis to be performed), charged and neutral particles in a predefined angular acceptance are grouped with the seed to form the jet. This approach was first developed at LEP by the OPAL Collaboration in Ref. [73]. This kind of algorithm is particularly useful for the reconstruction of long-lived hadron jets. The purities in terms of b-hadron (or c-hadron) decay tracks and measured b-hadron (or c-hadron) energy of the subsequent jet are improved with respect to that obtained with JADE based algorithms (see Ref. [74]). The best angular resolution for the b-hadron flight direction is achieved with this algorithm.

5.3 Lepton identification

In this thesis, a *lepton* refers to an electron or a muon. Their typical decay length being much larger than the dimensions of the detector (∞ for electrons, 300 Km for muons), they are reconstructed as charged particles in the tracking detectors, and identified from their typical interaction in all subdetectors (TPC, ECAL, HCAL, and muon chambers) as described in Section 4.2 and in Ref. [66].

All tracks considered by the hadronic selection described in the previous Section are taken as possible lepton candidates. As a first step of the lepton identification, some additional track-quality cuts are applied. *i*) At least five TPC hits are required; *ii*) the distance of closest approach to the beam axis must be smaller than 5 mm; and *iii*) and the z-coordinate of the track at the point of closest approach must be, in absolute, smaller than 5 cm.

In the following Sections the electron and muon specific selection criteria and performance are given.

5.3.1 Electron identification

The electron identification makes use of the ionization measurement in the TPC and the shape of the electromagnetic shower developed in the ECAL. These basic measurements are expressed in terms of normally distributed estimators on which cuts are applied to select electron candidates. The redundancy of the TPC and the ECAL information allows the performance of each estimator to be evaluated directly with the data.

Electron candidates are first required to have a momentum greater than $2\,\mathrm{GeV}/c$. The electron hypothesis is tested in the TPC and ECAL with a procedure as follows.

Electron identification in the TPC

For each track in the TPC, the $\mathrm{d}E/\mathrm{d}x$ is measured from the wires and from the pads. The measurement from the wires is more precise, but it is reliable only if at least fifty wire hits are associated with the track. The pads measurement is always available, it is combined with the wire estimate [68]. The combined $\mathrm{d}E/\mathrm{d}x$ estimator of the measured ionization in the TPC is normalized to 1.0 for a minimum-ionizing particle.

The $\mathrm{d}E/\mathrm{d}x$ estimation of each track is compared with its value expected in the electron-mass hypothesis, $\langle \mathrm{d}E/\mathrm{d}x \rangle_\mathrm{e}$. The final estimator is given by R_I

$$R_\mathrm{I} = \frac{\mathrm{d}E/\mathrm{d}x - \langle \mathrm{d}E/\mathrm{d}x \rangle_\mathrm{e}}{\sigma_{\mathrm{d}E/\mathrm{d}x}} \,, \tag{5.3}$$

where $\sigma_{\mathrm{d}E/\mathrm{d}x}$ is the one standard deviation resolution on the ionization measurement for the electron mass hypothesis. For a pure sample of electrons, the distribution of R_I is very close to a Gaussian of mean zero and width one. In this thesis, the cut applied on the R_I estimator to select electrons is $R_\mathrm{I} > -2.0$. No cut is applied to the positive R_I tail because only electrons are found in that region.

Electron identification in the ECAL

Both the compactness of the electromagnetic energy deposition around the particle direction reconstructed in the TPC, and the longitudinal shape of the shower, distinguish electrons from other particles, and are exploited for their identification.

All good tracks are extrapolated from the end of the TPC through the ECAL. A crossing point is computed at each of the three ECAL stacks.

The shower transverse development in the ECAL is measured with the estimator R_T. This estimator is defined from the track momentum, p, and the energy deposited, E_4, in the four towers closest to the extrapolated track, E_4

$$R_\mathrm{T} = \frac{E_4/p - \langle E_4/p \rangle}{\sigma_{E_4/p}} \,, \tag{5.4}$$

where $\langle E_4/p \rangle$ is the expected value of E_4/p for an electron, and $\sigma_{E_4/p}$ is the expected resolution (one standard deviation). The R_T estimator is most efficient for hadron rejection when the momentum of the track is high.

The longitudinal shower development is expressed with the estimator $R_{\rm L}$. The inverse of the first moment of the longitudinal energy distribution is defined by

$$\chi_{\rm L} \;=\; \frac{E_4}{\sum\limits_{i=j}^{4}\sum\limits_{j=1}^{3} E_i^j S_j} \;, \tag{5.5}$$

where E_i^j is the energy deposited in the i-th storey of the j-th stack, and S_j is the mean depth of the energy deposits in the j-th stack. The quantity $\chi_{\rm L}$ is independent of the angle of the incoming particle and it is computed using the energy measured in the three stacks with an iterative procedure assuming, at each step, that the longitudinal deposition induced by an electromagnetic shower is described by the standard shape [75]. This procedure converges quickly for electrons and it is essentially divergent for hadrons. The longitudinal estimator reads

$$R_{\rm L} \;=\; \frac{\chi_{\rm L} - \langle\chi_{\rm L}\rangle}{\sigma_{\chi_{\rm L}}} \;, \tag{5.6}$$

and has a normal Gaussian distribution for electrons.

The distribution of $R_{\rm T}$ versus $R_{\rm L}$ for a sample of tracks enriched in photon conversions is shown in Fig. 5.1. The electron and hadron contributions are clearly separated, the accu-

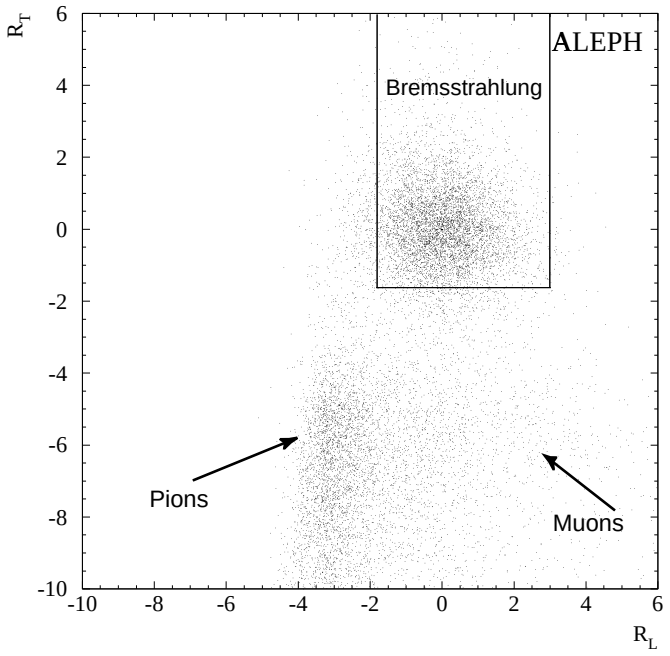

Figure 5.1: The ECAL estimators for a sample of electrons from photon conversions in the data.

mulation of events around $R_{\rm T} = 0$ and $R_{\rm L} = 0$ is due to electrons. The following cuts are optimized to maximize hadron rejection with a limited efficiency loss:

$$\begin{aligned} -1.8 \;&<\; R_{\rm L} < 3.0 \;, \\ -1.6 \;&<\; R_{\rm T} \;. \end{aligned} \tag{5.7}$$

No upper cut is applied on the R_{T} estimator because the four central towers associated to an electron can contain additional energy from a Bremsstrahlung photon, thus increasing the measured value of R_{T}. The region delimited by the cuts in R_{L} and R_{T} is shown in Fig. 5.1.

Electron identification performance

The simultaneous use of the three estimators described above provides an electron identification efficiency in jets independent of the transverse momentum of the electron candidate with respect to its jet. A dependence on the track momentum is observed, the efficiency decreases with momentum. The electron identification efficiency, computed after the momentum and R_{T}, R_{L} cuts, is 98.9% with a purity of 94.4%. The most important contamination to the electron candidate sample comes from pions, which account for $\sim 90\%$ of it.

5.3.2 Muon identification

Muons are identified by the tracking capabilities of the hadron calorimeter, together with the muon chamber information. The TPC $\mathrm{d}E/\mathrm{d}x$ estimator can be used as well to further reject misidentified charged kaons.

To identify muons in the HCAL, a 'road' is opened around the track extrapolated, with a width of three times the estimated extrapolation uncertainty due to multiple scattering in the calorimeter material. The number of hits in each of the 23 HCAL planes of streamer tubes is counted. In each of these planes, a muon is expected to leave one hit if the 'road' intersects it within an active region, the plane is said to have fired if a digital hit lies within the multiple scattering 'road'. The number of expected hits is then compared to the observed number. Tracks are considered for muon identification in hadronic events if their momentum is greater than $2.5\,\mathrm{GeV}/c$, which ensures that all muons exit the muon chambers, and that the identification efficiency does not vary significantly with momentum.

The cuts used to define a muon are

- $N_{\mathrm{fir}}/N_{\mathrm{exp}} \geq 0.4$;
- $N_{\mathrm{exp}} \geq 10$;
- $N_{10} > 4$;

where N_{exp}, N_{fir}, and N_{10} are, respectively, the number of planes expected to be hit by a muon, the number of planes actually hit, and the number of planes hit within the last expected ten. These cuts are well suited for isolated muons. In order to enhance the rejection power against hadrons in jets, the typical features of the digital pattern created by a hadron shower in the HCAL are used. A variable, X_{mult}, is computed by counting all the HCAL digital hits in the last eleven planes within a wider 'road' around the extrapolated track. The result is divided by the number of fired planes so that X_{mult} represents the average hit multiplicity per fired plane. For muon identification it is requested to be smaller than 1.5.

In Fig. 5.2, the distributions of $N_{\mathrm{fir}}/N_{\mathrm{exp}}$, N_{10}, and X_{mult} for muons from $\mathrm{Z} \to \mu^+\mu^-$ events are compared to those of pions produced in τ decays.

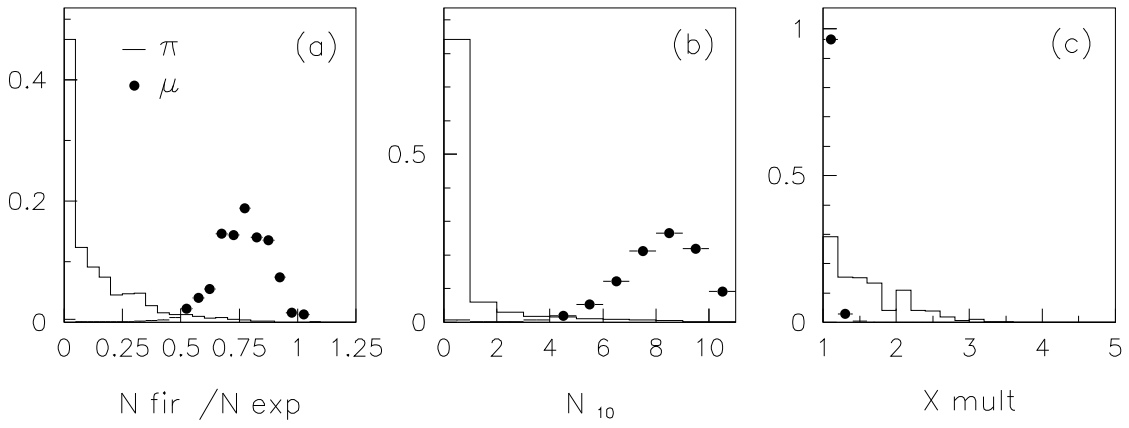

Figure 5.2: Distribution of (a) $N_{\rm fir}/N_{\rm exp}$, (b) N_{10}, and (c) $X_{\rm mult}$, for muons (points) and pions (solid line), with $N_{\rm exp} > 10$. The plots have been normalized to equal areas, and the vertical scale is arbitrary.

A track is defined to have hit a muon chamber if at least one of the two tube planes yields a space point whose distance from the extrapolated track is less than four times the estimated standard deviation from multiple scattering.

The requirement for the association of a muon chamber hit in addition to the HCAL muon criteria is very powerful for background rejection. The simulation predicts that, while about 94% of the muons identified in HCAL are associated to a muon chamber hit, only about 20% of the misidentified hadrons have this association.

A rejection cut against charged kaons which do not decay in the TPC can be applied to the TPC $\mathrm{d}E/\mathrm{d}x$ estimator with the muon-mass hypothesis, $R_{\rm I}(\mu)$,

$$R_{\rm I}(\mu) = \frac{\mathrm{d}E/\mathrm{d}x - \langle \mathrm{d}E/\mathrm{d}x \rangle_\mu}{\sigma_{\mathrm{d}E/\mathrm{d}x}} > -2\,. \tag{5.8}$$

In the ALEPH track reconstruction, kinks are identified as tracks for which a double helix fit with a common kink vertex point is better than a single helix fit. Those muon candidates which present a kink in the TPC are rejected. The purity on prompt muons is increased by 1%, with a negligible loss in efficiency.

The muon identification efficiency above $2.5\,\mathrm{GeV}/c$ is higher than 90% for a purity between 80% and 85%, with a mild dependence on the momentum. The most important contribution to the contamination comes from pions.

5.4 Primary vertex finding

The first step of the reconstruction of an event topology is the determination of the interaction point of the incoming $\mathrm{e^+e^-}$, the primary vertex. Some analyses, like those described in this thesis, need a three-dimensional position measurement with an accuracy better than $100\,\mu$m.

The performance achieved by the ALEPH tracking can be used to compute the primary vertex event by event using the reconstructed charged particles, and therefore improve on the precision of the LEP beam spot.

It is important that the algorithm chosen for the primary vertex determination has similar performance for all type of events. Some of the particles produced in a Z-boson decay, those which contain c- and b-quarks in particular, travel some distance from the interaction point through the detector volume before decaying in a heavy-hadron decay point. These particles are known as long-lived. In the presence of such particles, not all tracks in the event come from the interaction point, and therefore care has to be taken to avoid a bias in its reconstruction.

The algorithm used in ALEPH [76] removes the lifetime information of tracks by projecting them on the plane perpendicular to the jet direction as illustrated in Fig. 5.3. The

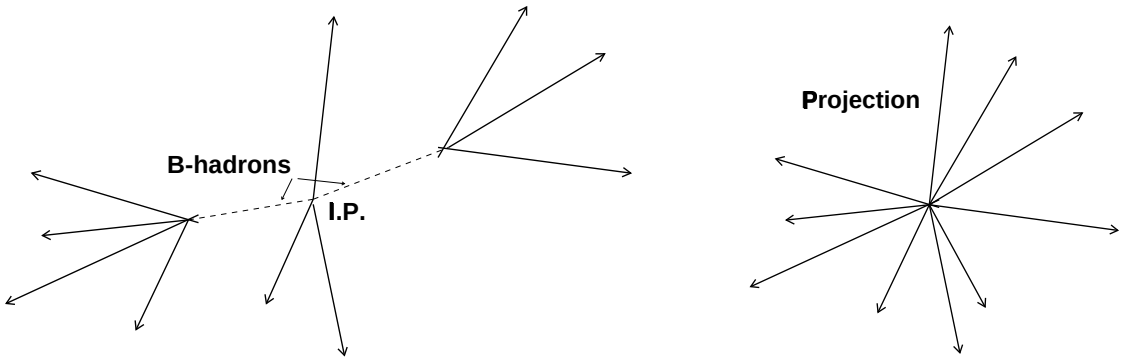

Figure 5.3: Schematic of a $Z \to b\overline{b}$ event on the left and its projection for primary vertex finding on the right

jet direction is chosen because it is a good approximation of the parent hadron direction. All tracks are projected onto the plane perpendicular to the direction of the nearest jet. The primary vertex is found in each of these planes, for each jet. The combination of the different projections of the primary vertex in each jet of an event is used to obtain the three-dimensional position of this vertex. The information from the LEP beam spot in the x-y direction is used as a constraint. A procedure to identify tracks which fit badly with the primary vertex is defined, and these tracks rejected from its determination. A correction to take into account the finite resolution on the jet direction is applied. As a final step, tracks with no lifetime are identified, and their information along the jet direction is used in the final primary vertex fit.

The algorithm is based on a χ^2 minimization, and at each of the step above, the uncertainty estimations are checked to give correct pull distributions. The core of the method relies on the first position estimation (before track rejection and other refinements) with the following χ^2 minimization with respect to V_i

$$\chi^2 = \sum_{i=1}^{3} \frac{(B_i - V_i)^2}{(\sigma_i^B)^2} + \sum_{j=1}^{N_{\text{jet}}} \sum_{k=1}^{N_{\text{track}}^j} \frac{(D_\perp^k)^2}{(\sigma_\perp^k)^2} \ , \tag{5.9}$$

where B_i is the beam spot position (from LEP) in the i- (x, y, or z) direction, σ_i^B is the size

of the beam envelope in the i-direction, $N_{\rm jet}$ is the number of jets in the event, $N^j_{\rm track}$ is the number of tracks in the j-th jet, $D^k_\perp$ is the distance between the vertex V and the track k on a plane perpendicular to the jet, and $\sigma^k_\perp$ is the uncertainty on that distance.

The typical resolution obtained for the primary vertex position depends on the type of events selected. It is of 30 μm, 10 μm, and 30 μm in the x, y, and z direction, respectively for $\mathrm{Z} \to \mathrm{u\overline{u}}$, $\mathrm{Z} \to \mathrm{d\overline{d}}$, or $\mathrm{Z} \to \mathrm{s\overline{s}}$, and 50 μm, 10 μm, and 60 μm for $\mathrm{Z} \to \mathrm{b\overline{b}}$ events.

5.5 Impact parameter

A jet axis is defined from the vector momenta of its particles and from the primary vertex position. Let S be the point of closest approach of a track to this axis. The distance D between the tangent of the track at the point S, and the primary vertex is called the impact parameter of the track with respect to the primary vertex. It is defined to have the same sign as the scalar product of $\vec{VS}$ and the jet direction. A schematic drawing of the impact parameter definition is given in Fig. 5.4. The uncertainty $\sigma_{\rm D}$ on the impact parameter is

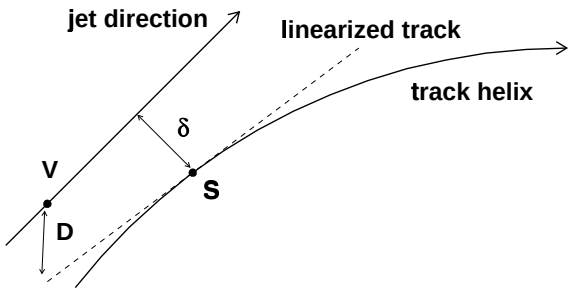

Figure 5.4: Impact parameter definition: V is the primary vertex, S is the point of closest approach of the track helix to the jet direction, δ is the jet-track distance, D is the impact parameter. The linearized track and the jet direction may lie in different planes. In this example, the track has a positive impact parameter.

calculated from the track fit covariance matrix, the primary vertex uncertainty, and their correlation. A non-zero correlation between the primary vertex position and the track fit parameters arises because tracks are used in the interaction point position estimate.

The impact parameter and its sign are used to identify charged particles with or without lifetime, *i.e.*, particles which are likely to come from the decay of a long-lived particle (such as a b-hadron) or not. Tracks with a negative impact parameter are likely to originate from the interaction point, whereas tracks issued from secondary vertices have a positive impact parameter. These properties are used for the selection of $\mathrm{Z} \to \mathrm{b\overline{b}}$ events, as explained in Section 5.7.

5.6 Inclusive secondary vertex finders

Examples of particles which end in a decay point separated from the interaction point are b-hadrons or c-hadrons, with a typical decay path of 3 mm and 2 mm respectively. The expected number of charged particles in the decay point of a b-hadron is five, and about five other charged particles are present on average from the fragmentation process. With as many tracks, the secondary vertex finding technique of forming a vertex from all possible track combinations is impracticable (because of the too large number of combinations) and a different approach must be followed. The aim of inclusive secondary vertex finder algorithms is to obtain an estimate of the decay position of these long-lived particles, without forming a vertex from all combinations of tracks. The algorithm does not provide a track-to-vertex association, instead, for each track, a probability of belonging to the decay vertex is given. Two such algorithms are used in ALEPH. The methods and the performance of both of them are explained in the following Sections.

5.6.1 QVSRCH

The QVSRCH algorithm [77] is based on a vertex search in a predetermined coordinate space, rather than a search among track combinations. For given primary and secondary vertex positions, a $\Delta\chi^2$ is defined as the difference between the χ^2 when all tracks are assigned to the primary vertex, and the sum of the primary and secondary vertex χ^2 values when some tracks are transferred from the primary to the secondary vertex. The maximum $\Delta\chi^2$ for fixed vertex coordinates is obtained by assigning each track to its closest vertex. The central idea in the algorithm is to calculate this $\Delta\chi^2$ for a grid in secondary vertex coordinate space, and determine the secondary vertex as the point of maximum $\Delta\chi^2$.

The event is divided in two jets and a secondary vertex is looked for in each of them. Two cylinders centred along both jet directions, with radius of 500 μm and length of 1 cm are defined. The $\Delta\chi^2$ is computed in every point of a grid in these cylinders (steps of 200 μm along the jet direction and 20 μm in the two orthogonal directions to it). The $\Delta\chi^2$ value between grid points is extrapolated from the values at the grid points with parabolic functions. These same functions are used to estimate the secondary vertex covariance matrix.

The way the algorithm is built guarantees a secondary vertex position to be obtained for most events, and therefore the efficiency on the decay length reconstruction is reasonably uniform as a function of the decay length (as seen later in Fig. 5.6). The impact parameter of each track with respect to the primary and secondary vertices is used to compute a probability of each track to belong to one or the other vertex. The maximum value of the $\Delta\chi^2$ gives an estimate of the vertex quality.

5.6.2 VNFIT

The VNFIT algorithm [78] is based on a likelihood fit which allows an arbitrary number of vertices for a set of tracks to be determined. The likelihood function used is the probability that the tracks are produced at a given number of vertices. A numerical maximization of this likelihood provides an estimate of a predetermined number of vertex positions as well as their uncertainties. The most common configuration for using this algorithm is to set

the number of vertices to three: the primary vertex (which can be given as input) and two secondary vertices for two b- or c-hadron decays (one in each hemisphere). Some additional constraints can be imposed, as the *a priori* knowledge of a track to come from a given vertex, for instance.

The likelihood value obtained after the maximization, assuming Gaussian uncertainties, is used to estimate the probability of the vertex as well as the probability of each track to come from its closest vertex.

Some differences are observed in the performance of the two algorithms described above. The second one, VNFIT, has the advantage to provide, on average, a slightly more accurate estimate of the decay point position. A comparison on the decay length resolution achieved for a common sample of simulated b-hadron decays with both algorithms is presented in Fig. 5.5.

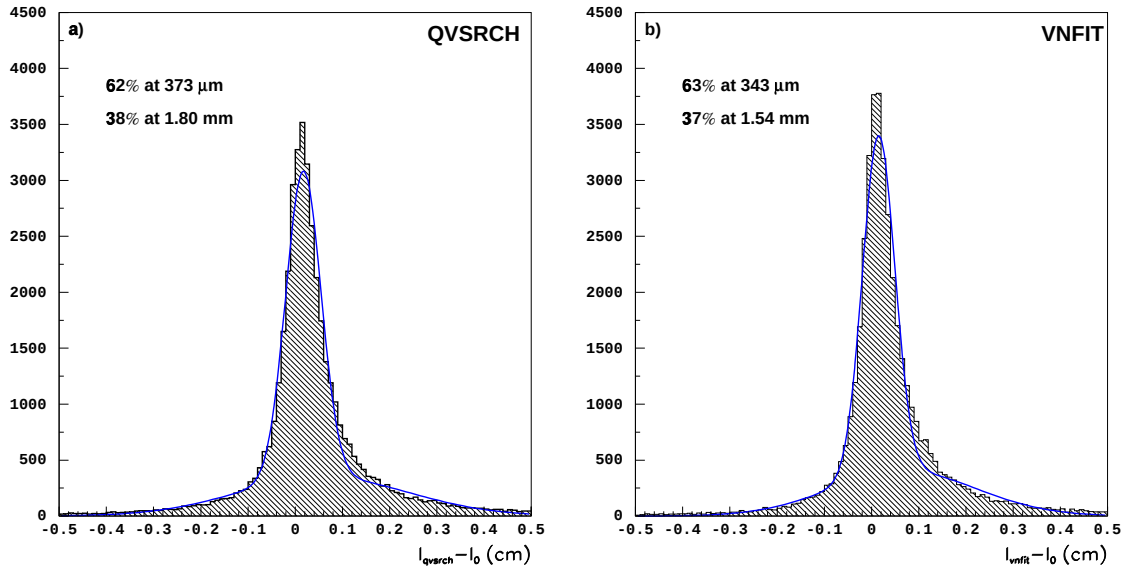

Figure 5.5: Decay length resolution for b-hadrons using a) QVSRCH, and b) VNFIT.

However, the QVSRCH algorithm is more efficient overall, in particular for b-hadron decay points close to the interaction point. The decay length reconstruction efficiency for both algorithms as a function of the decay length is shown in Fig. 5.6.

The two algorithms can therefore be used complementarily to obtain the best possible performance. For those decays for which VNFIT provides a secondary vertex position, this position and its uncertainty estimates are considered, the QVSRCH estimates are taken otherwise.

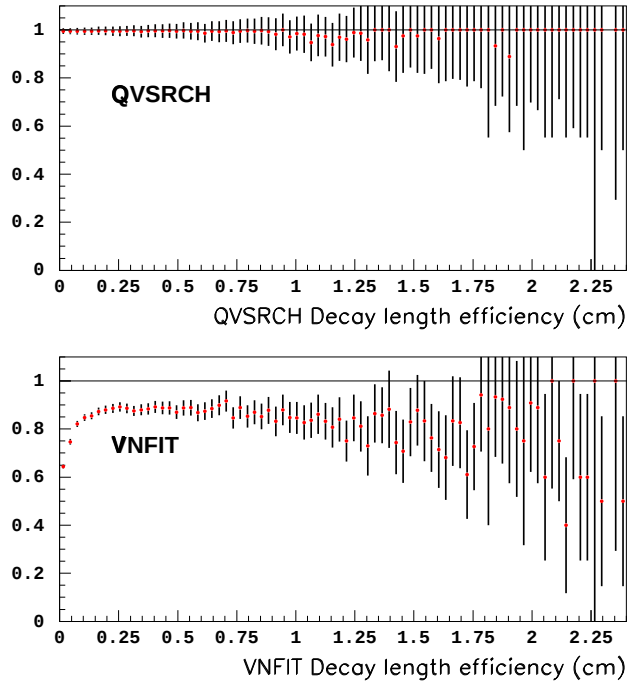

Figure 5.6: Decay length reconstruction efficiency as a function of the decay length for QVSRCH and VNFIT algorithms.

5.7 General b tagging

The aim of "b tagging" is to identify $Z \to b\overline{b}$ decays in a sample of $Z \to q\overline{q}$. The basic characteristics which distinguish $Z \to b\overline{b}$ decays from the other hadronic Z-boson decays are the large lifetime and the large mass of b-hadrons compared to those of other particles produced in $Z \to q\overline{q}$ decays.

Different approaches are possible for "b tagging": from the complete reconstruction of specific b-hadron decays on one side, to fully inclusive tagging where no specific b-hadron, nor decay, are identified, on the other. It is also possible to use the leptonic spectrum properties for the selection of semileptonic b-hadron decays. In this Section only generic selection methods used in ALEPH are described.

5.7.1 QIPBTAG

The QIPBTAG (Ref. [79]) algorithm exploits the non-zero b-hadron lifetime. The signature of a b-hadron is the presence of charged particles in the event which do not originate from the interaction point. In this algorithm the secondary decay vertex is not reconstructed. Instead, the signed impact parameter of all tracks from the Z-boson decay is used (the impact parameter definition, its sign and its uncertainty are given in Section 5.5).

The main idea of the algorithm is to use all tracks with lifetime information (*i.e.*, with significant impact parameter with respect to the interaction point), either coming directly

from the b-hadron decay point or, in the typical case where the b-hadron decays to a c-hadron, coming from the decay point of the c-hadron. A track selection (slightly more restrictive than that described in Section 5.1) based on the quality of the track reconstruction is applied, and the signed impact parameter is computed for all selected tracks. Only tracks with positive impact parameter are considered for the "b-tagging" estimator computation. Tracks with negative impact parameter are used as a calibration sample as they constitute an almost pure set of tracks originated from the interaction point (the contamination of tracks originating from a secondary vertex in that sample is typically about 1%).

The statistical resolution on the impact parameter varies strongly as a function of the charged particle momentum, angle, and number of VDET hits. It is therefore difficult to interpret the value of the impact parameter itself. Instead, the algorithm uses the impact parameter significance, $\mathrm{D}/\sigma_{\mathrm{D}}$. The resolution function for $\mathrm{D}/\sigma_{\mathrm{D}}$ is measured on the calibration sample, and it is used to define the probability, $\mathcal{P}_t$, that a track with positive measured $\mathrm{D}/\sigma_{\mathrm{D}}$ originates from the interaction point.

Given a group of N tracks with positive impact parameter, the combined b-tagging estimator is defined as

$$\mathcal{P}_N \;=\; z \sum_{j=0}^{N-1} \frac{(-\ln z)^j}{j!} \;, \tag{5.10}$$

where $z \equiv \prod_{i=1}^{N} \mathcal{P}_{t_i}$, so as to give a uniform distribution of $\mathcal{P}_N$ between zero and one, for events without lifetime.

Small values of the combined estimator indicate low probability of the tracks to all come from the interaction point, and therefore a high probability that they belong to a $\mathrm{Z} \to \mathrm{b\overline{b}}$ decay. In Fig. 5.7, the value of the estimator computed with all selected tracks in each event is displayed; on Fig. 5.7a for simulated events with a Z-boson which decays into a light-quark pair, $\mathrm{u\bar{u}}$, $\mathrm{d\bar{d}}$, or $\mathrm{s\bar{s}}$, and on Fig. 5.7b for $\mathrm{Z} \to \mathrm{b\overline{b}}$ decays. For a generic cut on the global estimator at 10^{-2}, an efficiency of 68% with a purity of 83% are obtained. The most important contamination comes from $\mathrm{c\overline{c}}$ events due to their lifetime; this contamination accounts for $\sim 14\%$ in the case of the previous cut.

5.7.2 QVSRCH

The inclusive vertex finder algorithm QVSRCH (Section 5.6.1), can be used to select $\mathrm{Z} \to \mathrm{b\overline{b}}$ decays as well. The relevant variable to distinguish $\mathrm{b\overline{b}}$ decays from the rest is the $\Delta\chi^2$ for the two secondary vertices found in the event.

Figure 5.8 shows the distribution of the sum of the two $\Delta\chi^2$ for $\mathrm{u\bar{u}}$, $\mathrm{d\bar{d}}$, and $\mathrm{s\bar{s}}$ in Fig. 5.8a and for and $\mathrm{b\overline{b}}$ simulated events in Fig. 5.8b. The requirement that $\Delta\chi^2$ be larger than 16 gives a $\mathrm{b\overline{b}}$ purity of 82% for an efficiency of 63%. The main background contribution, as in the case of QIPBTAG, comes from $\mathrm{c\overline{c}}$ events which contribute 67% of the total contamination.

5.7.3 Mass tag: QBMTAG

The QBMTAG algorithm exploits the b-hadron mass, larger than that of other hadrons produced in Z-boson decays, and allows the b-purity of the selected sample to be further

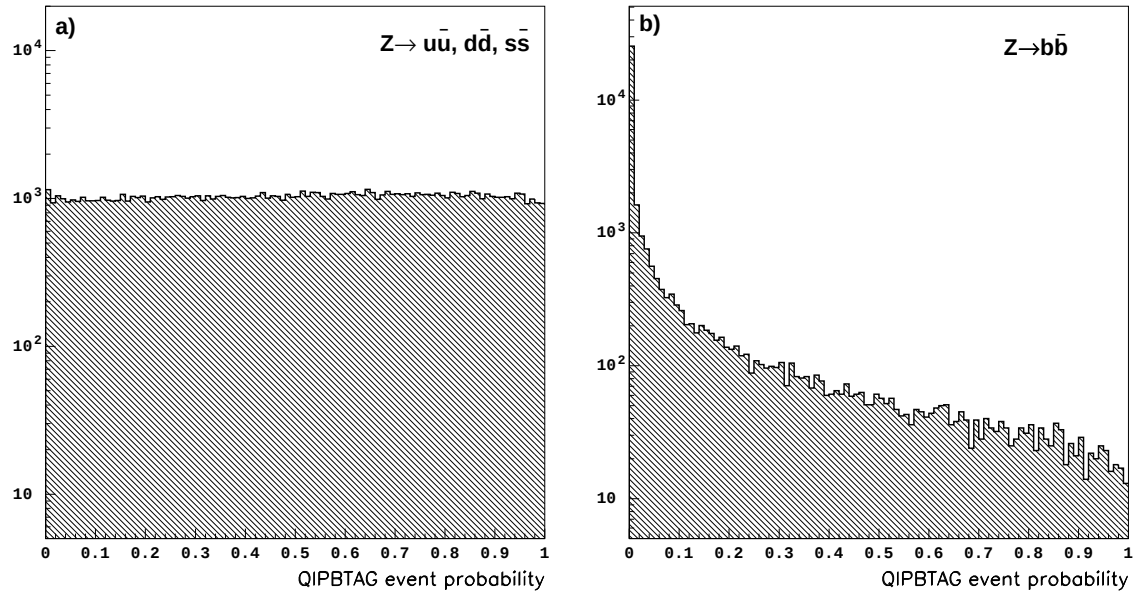

Figure 5.7: QIPBTAG estimator for a) $Z \rightarrow u\bar{u}, d\bar{d}, s\bar{s}$, and b) $Z \rightarrow b\overline{b}$ simulated events.

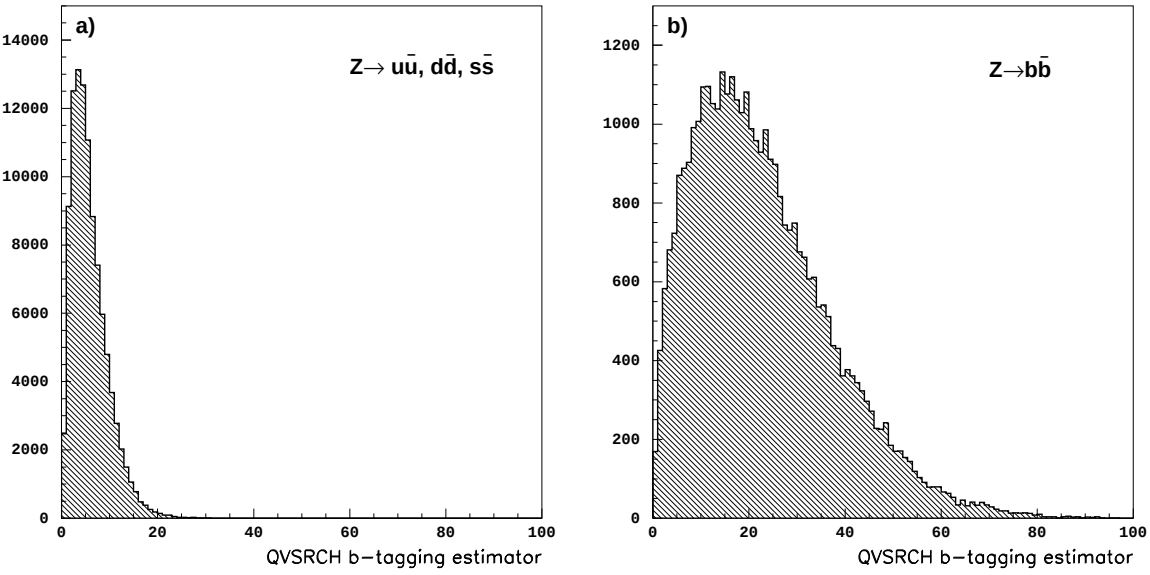

Figure 5.8: QVSRCH b-tagging estimator distribution for a) $Z \rightarrow u\bar{u}, d\bar{d}, s\bar{s}$, and b) $Z \rightarrow b\overline{b}$ simulated events.

increased.

For each hemisphere, tracks are ordered from the least to the most consistent with originating from the interaction point. The first tracks are grouped to form a c-hadron, *i.e.*, a particle with an invariant mass below $1.8\,\mathrm{GeV}/c^2$. The probability of the last track of this group to come from the interaction point, $\mathcal{B}_t$, is taken as b-tag estimator for the hemisphere. The track ordering may follow either the QIPBTAG or the QVSRCH scheme.

In Fig. 5.9a, the distribution of, $-\log_{10}(\mathcal{B}_t)$, is shown for hemispheres in $u\bar{u}$, $d\bar{d}$, and $s\bar{s}$ simulated events, and in Fig. 5.9b for $Z \to b\bar{b}$ hemispheres (for illustration the track ordering was taken from the QIPBTAG algorithm).

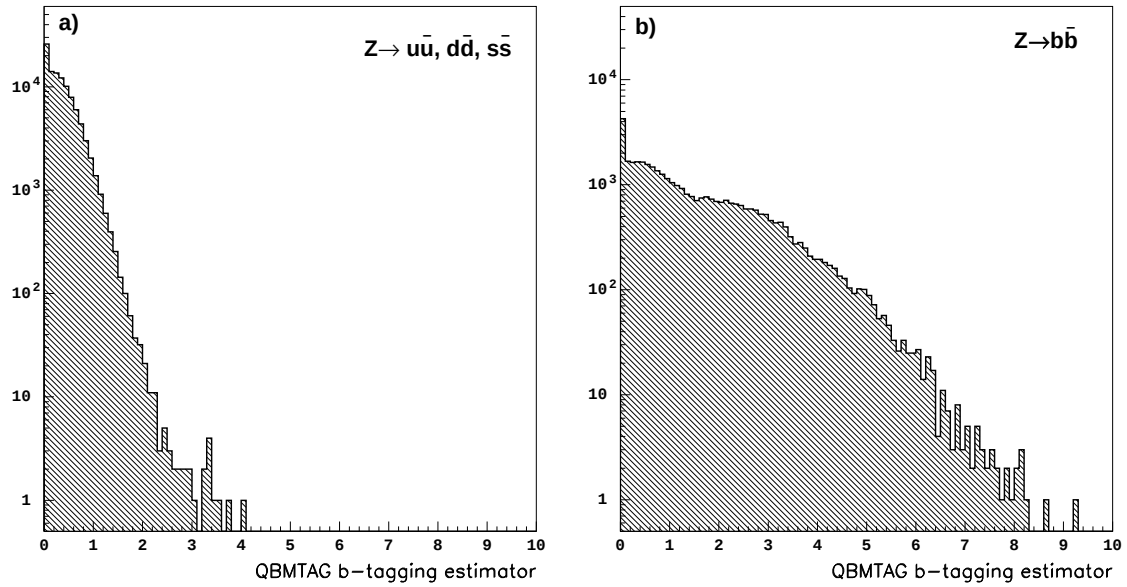

Figure 5.9: QBMTAG estimator distribution for $Z \to, u\bar{u}, d\bar{d}, s\bar{s}$, and b) $Z \to b\bar{b}$ simulated events.

A combination of the QBMTAG estimator on an event with either QIPBTAG or QVSRCH allows a purer $Z \to b\bar{b}$ sample to be selected. Typically values of a 98% $b\bar{b}$ purity and an efficiency of 40% can be achieved.